

A unified projection formalism for the Al-Pd-Mn quasicrystal Ξ -approximants and their metadislocations

M. Engel and H.-R. Trebin

Institut für Theoretische und Angewandte Physik, Universität Stuttgart,
Pfaffenwaldring 57, D-70550 Stuttgart, Germany
email: mengel@itap.physik.uni-stuttgart.de

June 23, 2021

Abstract

The approximants ξ , ξ' and ξ'_n of the quasicrystal Al-Mn-Pd display most interesting plastic properties as for example phason-induced deformation processes (KLEIN, H., AUDIER, M., BOUDARD, M., DE BOISSIEU, M., BERAHA, L., and DUNEAU, M., 1996, *Phil. Mag. A*, **73**, 309.) or metadislocations (KLEIN, H., FEUERBACHER, M., SCHALL, P., and URBAN, K., 1999, *Phys. Rev. Lett.*, **82**, 3468.). Here we demonstrate that the phases and their deformed or defected states can be described by a simple projection formalism in three-dimensional space - not as usual in four to six dimensions. With the method we can interpret microstructures observed with electron microscopy as phasonic phase boundaries. Furthermore we determine the metadislocations of lowest energy and relate them uniquely to experimentally observed ones. Since moving metadislocations in the ξ' -phase can create new phason-planes, we suggest a dislocation induced phase transition from ξ' to ξ'_n . The methods developed in this paper can as well be used for various other complex metallic alloys.

1 Introduction

A large number of periodic and quasiperiodic phases have been observed in the ternary Al-Pd-Mn system (Klein, Durand, and Audier 2000). Apart from the stable icosahedral phase (i-phase) there is a stable decagonal phase (d-phase) with 1.2 nm periodicity and a metastable d-phase with 1.6 nm periodicity, found by Tsai et al. (1991). The orthorhombic Ξ -approximants (ξ , ξ' and ξ'_n) of the i-phase form a class of closely related periodic phases and can be viewed as approximants of this 1.6 nm d-phase, as they have the following features in common with the d-phase:

- (a) They are arrangements of columns of Mackay-type clusters and intermediary atoms (Sun and Hiraga 1996). These clusters consist of about 52 atoms, placed on concentric shells of icosahedral symmetry as shown for the ξ' -phase by Boudard et al. (1996).
- (b) The columns are in registry, i.e. the compounds also have a layer structure.

The clusters contain about 80% of the atoms. Therefore a coarsened structural description makes sense where only the projections of the cluster columns along the column lines are marked. They lead to two-dimensional tilings, which are characteristic for the respective approximant phase. The vertices of the tiles correspond to the projections of the cluster columns.

The tilings contain flattened hexagons, which for the ξ -phase are aligned parallel (figure 1(a)), for the ξ' -phase are staggered in two orientations (figure 1(b)). In the ξ' -phase isolated combinations of a pentagon and a banana-shaped nonagon (figure 1(c)) are observed, along which the orientation of the hexagons is inverted and which are able to move by flips. Klein et al. (1996) therefore have termed them *phason-lines*, following the notation of related defects in quasicrystals. In bending experiments these phason-lines order into periodically aligned *phason-planes* with $1, 2, \dots, n$ rows of hexagons in between (figure 1(d) and (e)), forming periodic superstructures. Here we propose to name these phases ξ'_2 -, ξ'_3 -, \dots , ξ'_{n+1} -phases, the reason for the index-shift being given later. Most observed is the ξ'_2 -phase, which is also known as Ψ -phase (Klein 1997).

The ξ'_n -phases can be considered striped defect lattices. The stripes, which are the phason-planes, can bend and move, varying their distances (Beraha et al. 1997). Klein et al. (1999) have observed dislocations in the stripe pattern and have called them *metadislocations*. They are the characteristic textures of partial dislocations in the basic tiling.

In this article we are developing a simplified projection formalism to describe all the Ξ -phases. It is derived from the hyperspace method of the quasiperiodic phases. As a consequence, phasonic degrees of freedom can exist in the Ξ -phases which allow movements of the phason-planes. We determine those hyperlattice Burgers vectors which label the partial dislocations of lowest energies and relate them to the Burgers vectors of the metadislocations. Indeed, these are the only ones which are observed. The charming feature of our formalism is that the simplest model is working in three space so that all steps are easily imaginable.

2 Geometrical models for i-Al-Pd-Mn and its approximants

The atomic positions for a quasicrystal can be described by decorating the lattice points of a periodic hypercrystal with atomic surfaces and marking the points where these are intersected by a planar cut space (cut-method). An equivalent method is the strip-method (Katz and Duneau 1986). Approximants are constructed by using inclined cut spaces (Duneau and Audier 1994). For a detailed explanation see also Gratias, Katz, and Quiquandon (1995).

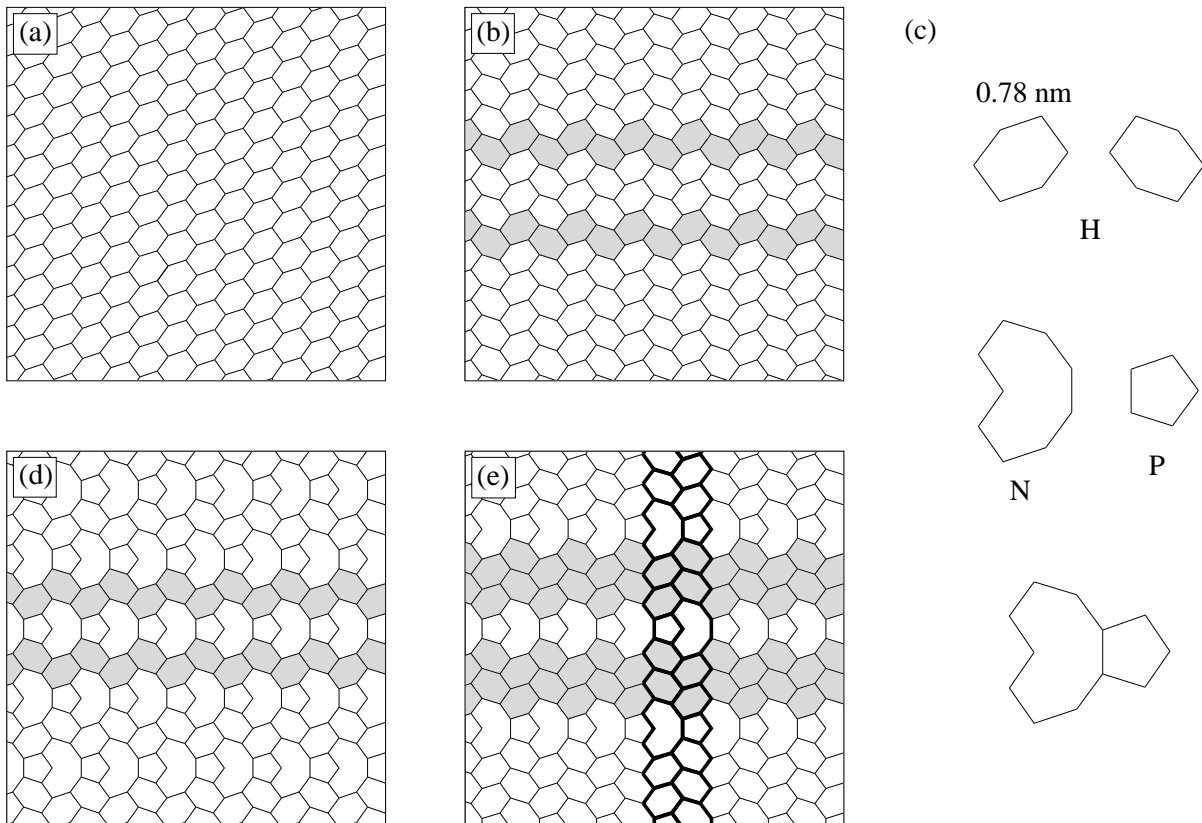


Figure 1: Tilings of four different approximant phases of the 1.6 nm d-phase. (a) Parallel alignment of hexagons in the ξ -phase. (b) Staggered arrangement of hexagons in the ξ' -phase. Two hexagon rows are marked grey. (c) The hexagons H occur in two different orientations. The other tiles, the pentagon P and the nonagon N can only be observed in combination, called phason-line. The edge length of the tiles is: $t^{6D} = 0.78$ nm. (d) In the ξ_2 -phase there is one row of hexagons between two phason-lines, also called phason-planes. (e) In the ξ_3 -phase there are two rows of hexagons between neighbouring phason-planes. The arrangement of hexagons is flipped at a phason-line as highlighted in the figure.

2.1 Sixdimensional cut-method for the i-phase and approximants

A six-dimensional hyperspace with orthogonal basis vectors $\mathbf{e}_1^{6D}, \dots, \mathbf{e}_6^{6D}$ of length $l^{6D} = 0.645$ nm was used by Katz and Gratias (1994) to model the i-phase of Al-Pd-Mn. The hyperspace was decorated with three different atomic surfaces positioned on different nodes in a face-centred lattice, namely

- even nodes: $n_0 = \{(z_1, \dots, z_6), z_i \in \mathbb{Z} \mid \sum_i z_i = 0 \pmod{2}\}$,
- odd nodes: $n_1 = \{(z_1, \dots, z_6), z_i \in \mathbb{Z} \mid \sum_i z_i = 1 \pmod{2}\}$,
- even body-centre nodes: $bc_0 = \{(z_1 + \frac{1}{2}, \dots, z_6 + \frac{1}{2}), z_i \in \mathbb{Z} \mid \sum_i z_i = 0 \pmod{2}\}$.

The cut space is spanned by three vectors, whose components in the above basis are ($\tau = \frac{1}{2}(\sqrt{5} + 1)$ is the golden mean):

$$\mathbf{a}_i^{6D} = (1, \tau, 0, -1, \tau, 0), \quad \mathbf{b}_i^{6D} = (\tau, 0, 1, \tau, 0, -1), \quad \mathbf{c}_i^{6D} = (0, 1, \tau, 0, -1, \tau). \quad (1)$$

Beraha et al. (1997) applied the cut-method for the three-dimensional atomistic description of the phases ξ and ξ' as approximants of the icosahedral phase. In order to position each single atom correctly, they had to modify the atomic surfaces slightly. It turned out that the centre volumes of the n_0 atomic surfaces, which lie again on a six-dimensional face-centred lattice, correspond to the cluster centre atoms. This way the model is reduced to three-dimensional tilings for the cluster positions only.

For the ξ' -phase Beraha et al. have derived the vectors that span a unit cell of the inclined cut space. We add the vectors for the inclined cut spaces of the ξ -phase and the ξ'_n -phases:

$$\mathbf{a}_\xi^{6D} = (0, 1, 1, -1, 0, 1), \quad \mathbf{b}_\xi^{6D} = \frac{1}{2}(5, 1, 1, 1, 1, -1), \quad \mathbf{c}_\xi^{6D} = (0, 0, 1, 1, -1, 1) \quad (2a)$$

$$\mathbf{a}_{\xi'}^{6D} = (0, 2, 1, -2, 1, 2), \quad \mathbf{b}_{\xi'}^{6D} = \mathbf{b}_\xi^{6D}, \quad \mathbf{c}_{\xi'}^{6D} = (0, 0, 1, 1, -1, 1) \quad (2b)$$

$$\mathbf{a}_{\xi'_n}^{6D} = (0, 2, 1, -2, 1, 2), \quad \mathbf{b}_{\xi'_n}^{6D} = \mathbf{b}_\xi^{6D}, \quad \mathbf{c}_{\xi'_n}^{6D} = (0, 0, 2n + 1, 2n, -2n - 1, 2n) \quad (2c)$$

The \mathbf{b}_ξ^{6D} -vector is the same for all the phases, because it marks the periodicity in the tenfold direction of the d-phase, which coincides with the column line of the Mackay-type clusters. By projecting in direction of \mathbf{b}_ξ^{6D} , two-dimensional tilings like those in figure 1 can be obtained. The edge length of the tiles is $t^{6D} = \frac{1}{5}\sqrt{10}\sqrt{\tau + 2}l^{6D} = 0.78$ nm. It can be calculated by projecting all connection vectors $\mathbf{e}_i^{6D} + \mathbf{e}_j^{6D}$ of neighbouring n_0 -sites onto the tiling plane. The shortest projections have length t^{6D} .

Since the six vectors \mathbf{a}_ξ^{6D} , \mathbf{c}_ξ^{6D} , $\mathbf{a}_{\xi'}^{6D}$, $\mathbf{c}_{\xi'}^{6D}$, $\mathbf{a}_{\xi'_n}^{6D}$ and $\mathbf{c}_{\xi'_n}^{6D} = 2n\mathbf{c}_{\xi'}^{6D} - \mathbf{a}_{\xi'}^{6D} + 2\mathbf{a}_\xi^{6D}$ lie in a three-dimensional subspace of the six-dimensional hyperspace, a description of the tilings in a three-dimensional hyperspace is possible by the cut-method. The model can be simplified by using a simple cubic lattice in three-space, as will be shown in detail in section 2.4. We can arrive at this conclusion directly after substituting the tiling of hexagons, pentagons and nonagons by a tiling of rhombs.

2.2 Rhombic substitution tiling

The new tiles are the thin and thick Penrose rhombs which in general are spanned by the vectors of a regular five-star. The interior angles of the tiles are multiples of 36° .

As shown in figure 2, a hexagon of the original tiling is substituted by a thick rhomb, and a nonagon/pentagon combination is substituted by a combination of a thin and a thick rhomb.¹ Therefore we will refer to the thin rhombs as phason-lines. A row of hexagons in staggered orientation is substituted by a row of alternating thick rhombs, and a phason-plane is substituted by a combination of a row of alternating thick rhombs and a row of thin rhombs, which again will be called phason-plane. Hence the number of rows of thick rhombs between two phason-planes in the new tiling for the ξ'_n -phase is exactly n .

Thus the tilings for the column positions of the Ξ -phases emerge as approximants of the Penrose tiling. However, only rhombs of three orientations show up. To span these only three prongs of the five-star are required. This is another argument why we can apply a projection formalism in a three-dimensional hyperspace which was mentioned above and is elaborated further below.

To model the lattices of all Ξ -phases, their phasonic degrees of freedom and their metadislocations we found it suitable to resort to a modified cut and projection method. To our knowledge it has not been applied yet in the literature. It makes use of *atomic hypervolumes* and requires a short section.

2.3 Atomic hypervolumes for a geometrical description in hyperspace

The method will be explained by the example of the well known one-dimensional Fibonacci-chain: The two-dimensional hyperspace is partitioned into equal unit cells, called atomic volumes (in general atomic hypervolumes) as shown in figure 3(a).² For the construction of an approximant, two different lines are needed: the cut line \mathcal{E} (in general cut plane or cut space) and the projection line E (in general projection plane or projection space, also named physical space). Those cells that are cut by \mathcal{E} are selected (marked grey). The middle point of those cells is projected onto the projection line.³ The projection leads to two different intervals on E , either a small one (S), when the neighbouring selected cells meet vertically, or a large one (L), when they meet horizontally, forming the tiles of the Fibonacci-chain.

¹A similar tiling has been presented by Klein et al. (1996). They used thick rhombs to model the ξ - and ξ' -phase and small hexagons for the phason-lines. However no description in hyperspace was presented, explaining the arrangement of the tiles.

²As a generalisation several overlapping atomic volumes could be used, as long as the number of times a point is covered is constant for the hyperspace. This way the closeness condition (Frenkel, Henley, and Siggia 1986) of the original cut-method is automatically fulfilled. But we will only make use of the method of atomic volumes for the canonical case of a hyper-cubic lattice \mathbb{Z}^n and the unit cells as atomic volumes.

³Any other choice is possible too, as long as it is the same point for each cell, since a different selection only leads to a global translation of the tiling.

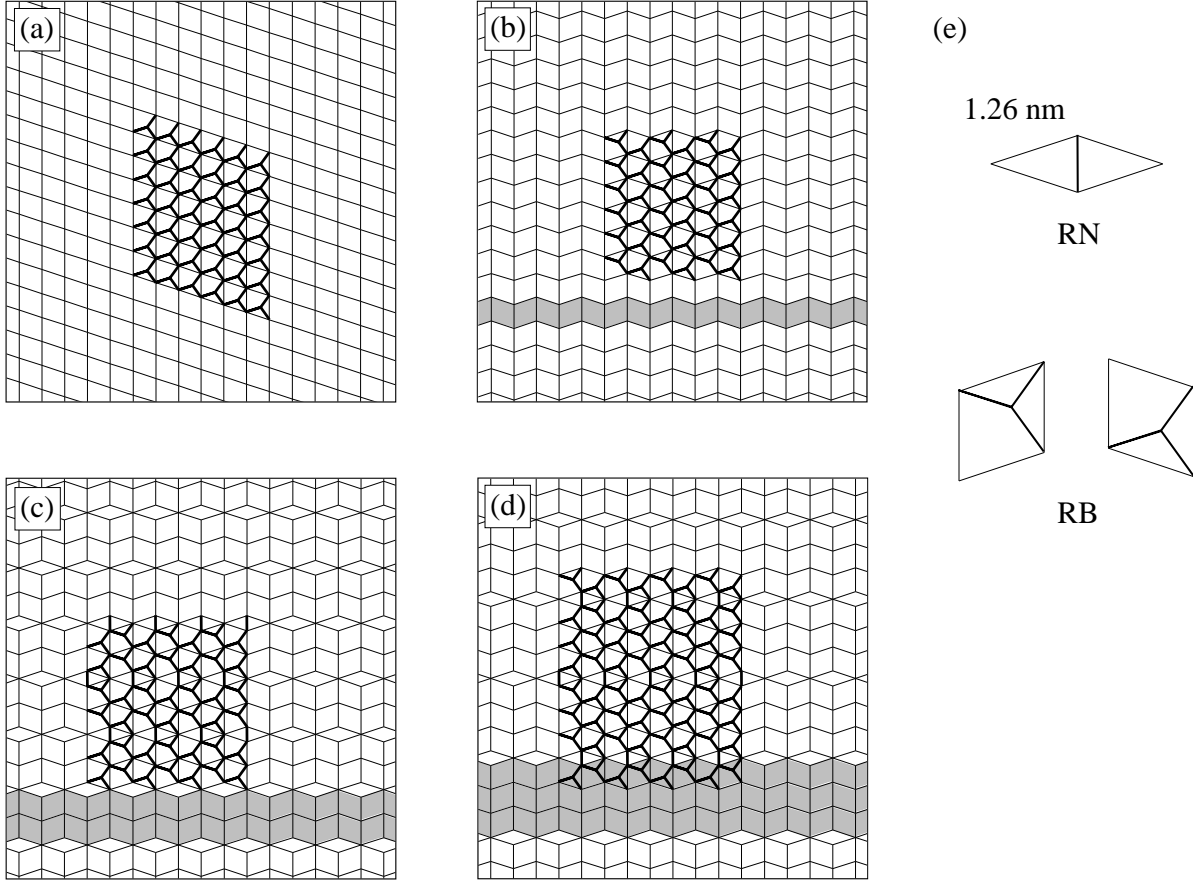


Figure 2: New tilings can be created by substituting the original tiles with thin Penrose rhombs RN, called phason-lines, and thick Penrose rhombs RB. The ξ -phase (a) and the ξ' -phase (b) are built only with the thick rhombs, while for the ξ'_2 -phase (c) and the ξ'_3 -phase (d) also the thin rhombs are needed. Between two phason-planes in the ξ'_n -phase there are n rows of alternating thick rhombs (marked grey). The new tiles are shown in (e). The edge length of the tiles is: $t^{5D} = 1.26$ nm.

The orientation of E determines the shape of the tiles. In the example of the Fibonacci-chain, it determines the ratio of S to L . In contrast, the orientation of \mathcal{E} fixes the arrangement of the tiles. Since different approximants of the same quasiperiodic phase are built from the same tiles, but with different arrangement of the tiles, the only difference in the construction is the varying orientation of \mathcal{E} . A rational slope of the cut line leads to a periodic tiling, while an irrational slope generates a quasiperiodic tiling. The special case of E and \mathcal{E} being identical is the original cut-method as mentioned above.

A geometrical restriction on the orientation of \mathcal{E} is imposed by the fact, that projected tiles must not overlap. In the example of the Fibonacci-chain this means, that the slope of \mathcal{E} must be positive. For a counterexample when it is not fulfilled see figure 3 (b). With this method we now construct the tilings of the cluster projections.

In the original cut-method the shape of the atomic surfaces depends on the orientation of the cut space. For the Fibonacci-chain the atomic surfaces are the projections of the unit cells on the orthogonal complement of \mathcal{E} . Because we will deal with cut spaces with spatially varying orientation in this paper, we would need a varying shape of the atomic surfaces as well. The method of atomic hypervolumes avoids these problems, as the atomic hypervolumes themselves do not vary.

2.4 Three- and five-dimensional hyperspace for approximants of Al-Pd-Mn

Because the rhombic tilings for the Ξ -phases are approximants of the Penrose tiling they can be described in a five-dimensional hyperspace with basis $\{\mathbf{e}_1^{5D}, \dots, \mathbf{e}_5^{5D}\}$, the hypercubic lattice \mathbb{Z}^5 and the unit cells as atomic hypervolumes. The projection plane of the Penrose tiling is spanned by the vectors

$$\begin{aligned}\mathbf{a}_p^{5D} &= (\sin(2\pi\frac{0}{5}), \sin(2\pi\frac{1}{5}), \sin(2\pi\frac{2}{5}), \sin(2\pi\frac{3}{5}), \sin(2\pi\frac{4}{5})), \\ \mathbf{c}_p^{5D} &= (\cos(2\pi\frac{0}{5}), \cos(2\pi\frac{1}{5}), \cos(2\pi\frac{2}{5}), \cos(2\pi\frac{3}{5}), \cos(2\pi\frac{4}{5}))\end{aligned}\quad (3)$$

and the projection matrix is obtained by writing these vectors normalised in the rows:

$$\pi_{\parallel}^{5D} = \frac{1}{5}\sqrt{10} \begin{pmatrix} \sin(2\pi\frac{0}{5}) & \sin(2\pi\frac{1}{5}) & \sin(2\pi\frac{2}{5}) & \sin(2\pi\frac{3}{5}) & \sin(2\pi\frac{4}{5}) \\ \cos(2\pi\frac{0}{5}) & \cos(2\pi\frac{1}{5}) & \cos(2\pi\frac{2}{5}) & \cos(2\pi\frac{3}{5}) & \cos(2\pi\frac{4}{5}) \end{pmatrix}. \quad (4)$$

The projections $\mathbf{f}_i = \pi_{\parallel}^{5D} \mathbf{e}_i^{5D}$ of the five-dimensional basis vectors give a regular five-star as drawn in figure 4(a). The rhomb tiles are the projection of two-dimensional faces of the five-dimensional unit cells. Each is spanned by two vectors of the five-star.

The edge length of the rhomb tiles can be calculated from the edge length of the pentagon/hexagon/nonagon-tiles as shown in figure 2(e): $t^{6D} = 2 \cos(72^\circ) t^{5D} = \tau t^{5D}$. This gives: $t^{5D} = \frac{1}{5}\sqrt{10} \tau \sqrt{\tau + 2} l^{6D} = 1.26$ nm, leading to the length of the basis vectors in the five-dimensional hyperspace: $l^{5D} = \tau \sqrt{\tau + 2} l^{6D} = 1.99$ nm.

A basis $\{\mathbf{a}^{5D}, \mathbf{c}^{5D}\}$ for the cut plane of a periodic approximant can be determined with a basis of the unit cell of the tiling. This is done in figures 4(b)-(e) for various approximant

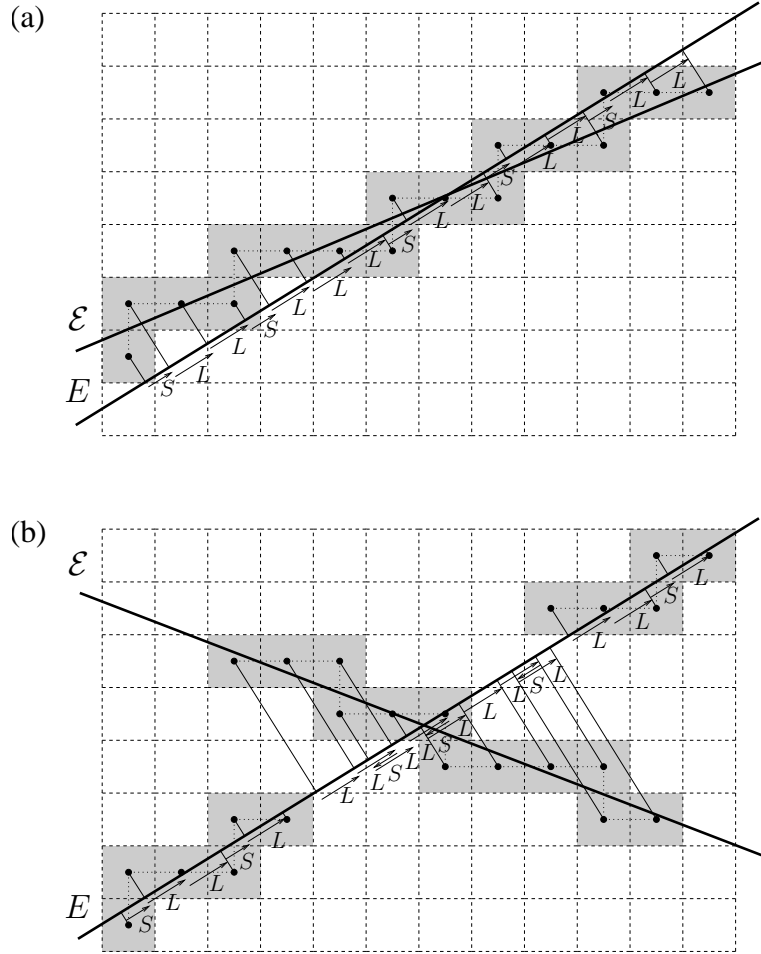


Figure 3: (a) Construction of an approximant of the Fibonacci-chain by the method of atomic volumes. A cut line \mathcal{E} and a projection line E are required (see text). (b) If the slope of \mathcal{E} is negative, the projected tiles overlap. This case is geometrically not allowed. In the bottom left and top right corner a small part of the quasiperiodic Fibonacci-chain is drawn.

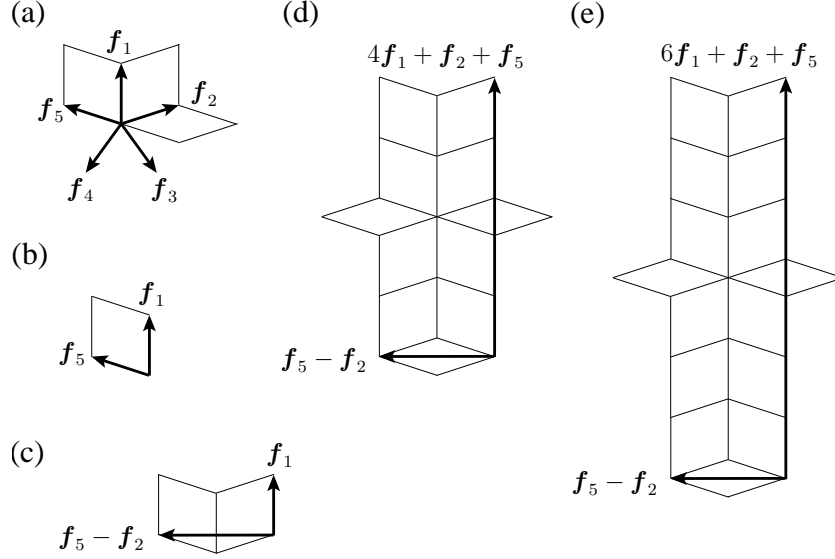


Figure 4: (a) The projected basis vectors \mathbf{f}_i lie on a regular five-star. The three rhombs of the tilings in figure 2 can be constructed with \mathbf{f}_1 , \mathbf{f}_2 and \mathbf{f}_5 . Unit cells of approximants and their bases are shown: the ξ -phase (b), the ξ' -phase (c), the ξ_2' -phase (d) and the ξ_3' -phase (e).

phases:

$$\mathbf{a}_\xi^{5D} = (0, 0, 0, 0, 1), \quad \mathbf{c}_\xi^{5D} = (1, 0, 0, 0, 0), \quad (5a)$$

$$\mathbf{a}_{\xi'}^{5D} = (0, -1, 0, 0, 1), \quad \mathbf{c}_{\xi'}^{5D} = (1, 0, 0, 0, 0), \quad (5b)$$

$$\mathbf{a}_{\xi_n'}^{5D} = (0, -1, 0, 0, 1), \quad \mathbf{c}_{\xi_n'}^{5D} = (2n, 1, 0, 0, 1). \quad (5c)$$

We now want to derive the transition matrix T_{5D}^{6D} from the five- to the six-dimensional hyperspace which maps the basis vectors \mathbf{a}^{5D} and \mathbf{c}^{5D} on \mathbf{a}^{6D} and \mathbf{c}^{6D} . The first column of T_{5D}^{6D} is fixed by the relation $\mathbf{c}_\xi^{6D} = T_{5D}^{6D} \mathbf{c}_\xi^{5D}$. The other columns follow from symmetry considerations. The fivefold rotation of the hyperspaces that fixes the projection plane is for the five- and six-dimensional model:

$$R^{5D} = \begin{pmatrix} 0 & 1 & 0 & 0 & 0 \\ 0 & 0 & 1 & 0 & 0 \\ 0 & 0 & 0 & 1 & 0 \\ 0 & 0 & 0 & 0 & 1 \\ 1 & 0 & 0 & 0 & 0 \end{pmatrix}, \quad R^{6D} = \begin{pmatrix} 1 & 0 & 0 & 0 & 0 & 0 \\ 0 & 0 & 1 & 0 & 0 & 0 \\ 0 & 0 & 0 & 1 & 0 & 0 \\ 0 & 0 & 0 & 0 & 0 & -1 \\ 0 & 1 & 0 & 0 & 0 & 0 \\ 0 & 0 & 0 & 0 & -1 & 0 \end{pmatrix}. \quad (6)$$

Observe, that R^{6D} does not change the vector \mathbf{b}_ξ^{6D} . The symmetry operation in the two hyperspace must match: $R^{6D} T_{5D}^{6D} = T_{5D}^{6D} R^{5D}$. This determines the $(i+1)$ -th column of T_{5D}^{6D} via

$$\mathbf{c}_\xi^{6D} = [R^{6D}]^{-i} \circ T_{5D}^{6D} \circ [R^{5D}]^i \mathbf{c}_\xi^{5D} \quad (7)$$

resulting in:

$$T_{5D}^{6D} = \begin{pmatrix} 0 & 0 & 0 & 0 & 0 \\ 0 & -1 & -1 & 1 & 1 \\ 1 & 0 & -1 & -1 & 1 \\ 1 & 1 & 0 & -1 & -1 \\ -1 & -1 & 1 & 1 & 0 \\ 1 & -1 & -1 & 0 & 1 \end{pmatrix}. \quad (8)$$

After fixing a coordinate system for the atomic hypervolumes in the five-dimensional hyperspace, the approximant phases can appear in five different orientations corresponding to a cyclic permutation of the basis vectors. Each orientation of the phases ξ' and ξ'_n is characterised by the orientation of the thin rhombs. By fixing their orientation, a lower-dimensional hyperspace can be used. Since the third and fourth components of the basis vectors in (5) vanish, a description in a *three-dimensional* hyperspace with cubic lattice \mathbb{Z}^3 (lattice parameter $l^{5D} = l^{3D}$) and the unit cell as atomic volume is possible by omitting these components. The transition matrix is simply:

$$T_{3D}^{5D} = \begin{pmatrix} 1 & 0 & 0 \\ 0 & 1 & 0 \\ 0 & 0 & 0 \\ 0 & 0 & 0 \\ 0 & 0 & 1 \end{pmatrix}. \quad (9)$$

For the Ξ -phases this three-dimensional model leads to the same tilings as the five-dimensional model, but only one orientation of the thin rhombs and two orientations of the thick rhombs can show up. The projection matrix π_{\parallel}^{3D} is derived from π_{\parallel}^{5D} again by omitting the third and fourth components:⁴

$$\begin{aligned} \pi_{\parallel}^{3D} &= \frac{1}{5}\sqrt{10} \begin{pmatrix} \sin(2\pi\frac{0}{5}) & \sin(2\pi\frac{1}{5}) & \sin(2\pi\frac{4}{5}) \\ \cos(2\pi\frac{0}{5}) & \cos(2\pi\frac{1}{5}) & \cos(2\pi\frac{4}{5}) \end{pmatrix} \\ &= \frac{1}{5}\sqrt{10} \begin{pmatrix} 0 & \frac{1}{2}\sqrt{2+\tau} & -\frac{1}{2}\sqrt{2+\tau} \\ 1 & \frac{1}{2}\tau^{-1} & \frac{1}{2}\tau^{-1} \end{pmatrix}. \end{aligned} \quad (10)$$

Bases for the cut planes in the three-dimensional model are given by

$$\mathbf{a}_{\xi}^{3D} = (0, 0, 1), \quad \mathbf{c}_{\xi}^{3D} = (1, 0, 0), \quad (11a)$$

$$\mathbf{a}_{\xi'}^{3D} = (0, -1, 1), \quad \mathbf{c}_{\xi'}^{3D} = (1, 0, 0), \quad (11b)$$

$$\mathbf{a}_{\xi'_n}^{3D} = (0, -1, 1), \quad \mathbf{c}_{\xi'_n}^{3D} = (2n, 1, 1). \quad (11c)$$

2.5 Relationships of the hyperspaces

So far the three- and five-dimensional hyperspace have been introduced only phenomenologically for the description of tilings of the approximant phases. Now we want to show

⁴This projection is not orthogonal, while the projection π_{\parallel}^{5D} is orthogonal. That is a consequence of the omission of two hyperspace dimensions.

how they are related to the original six-dimensional hyperspace. This is meant as a clarification of hyperspace geometry. Mathematically, the formation of the approximants from the icosahedral quasicrystal proceeds in two steps:

- (i) The configuration in direction of a fivefold rotation axis \mathbf{b} is changed, while the configuration perpendicular to this direction in the plane spanned by \mathbf{a} and \mathbf{c} is unaltered, leading to a pentagonal or decagonal quasicrystal. This step cannot be described simply by a reorientation of the cutplane. Additionally a relaxation of the atoms in direction of \mathbf{b} is necessary as shown by Beraha et al. (1997).
- (ii) The configuration in the plane spanned by \mathbf{a} and \mathbf{c} is changed, while the configuration in direction of \mathbf{b} is unaltered. This step is accurately described by a reorientation of the cutplane as used in this paper.

In step (i) a fivefold symmetry of the icosahedral quasicrystal is conserved. The fivefold rotation R^{6D} (equation (6)) operates trivially on a two-dimensional subspace U_1 spanned by $(1, 0, 0, 0, 0, 0)$, $(0, 1, 1, 1, 1, -1)$ and as a true rotation on the four-dimensional orthogonal complement U_2 spanned by $(0, 0, 1, 1, -1, 1)$, $(0, -1, 0, 1, -1, -1)$, $(0, -1, -1, 0, 1, -1)$, $(0, 1, -1, -1, 1, 0)$. So for quasicrystals and approximants the lattice vector \mathbf{b} is projected from U_1 , and the vectors \mathbf{a} and \mathbf{c} are projected from U_2 .

The restriction of \mathbb{Z}_6 onto U_2 leads to a non-cubic four-dimensional lattice (the \mathbb{A}_4 root lattice) that could in principle be used for the construction of the Penrose tiling and its approximant tilings. By adding a one-dimensional complementary space Δ , these tilings can be constructed from the \mathbb{Z}^5 -lattice. This is well-known and the usual way to describe the Penrose lattice. The relation of the five-dimensional hyperspace to the three-dimensional hyperspace is described in section 2.4. Figure 5 summarizes all the hyperspace relationships.

3 Phasonic degrees of freedom

Besides standard elastic (*phononic*) degrees of freedom, quasicrystals have additional degrees of freedom (Socolar, Lubensky, and Steinhardt 1986), which originate from the fact that the cut space is embedded in hyperspace. Local *excitations* of these so-called *phasonic* degrees of freedom, correspond to continuous displacements of the cut space along the direction orthogonal to it in hyperspace. The direction of the excitation is understood as the direction of the displacement.

The number of the phasonic degrees of freedom for a n -dimensional hyperspace and a d -dimensional cut space is equal to $n - d$. As will be shown, phasonic degrees of freedom are also possible for approximant phases, although then they are not any more continuous degrees of freedom. For convenience we nonetheless continue using this notation.

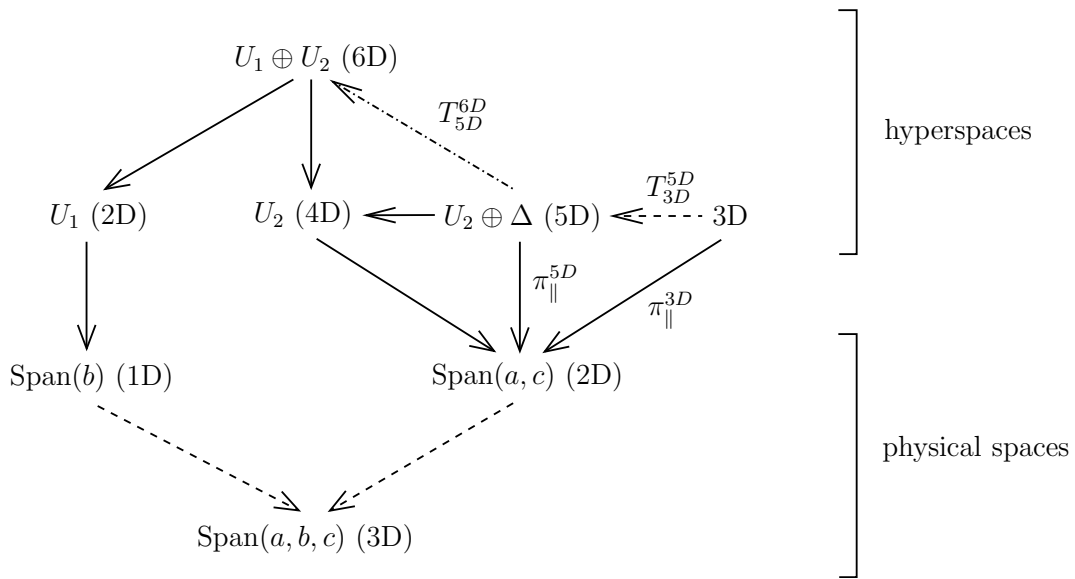


Figure 5: Relationship of the hyperspaces and the physical spaces. The five-dimensional space is built on top of the four-dimensional space U_2 perpendicular to the fivefold two-dimensional plane U_1 . It is not a (full) subspace of the original six-dimensional space. Solid arrows indicate projections (subspace relationship). Dashed arrows indicate inclusions. $T_{5D}^{6D}|_{U_2}$ is an inclusion and $T_{5D}^{6D}|_{\Delta} = 0$ the zero mapping.

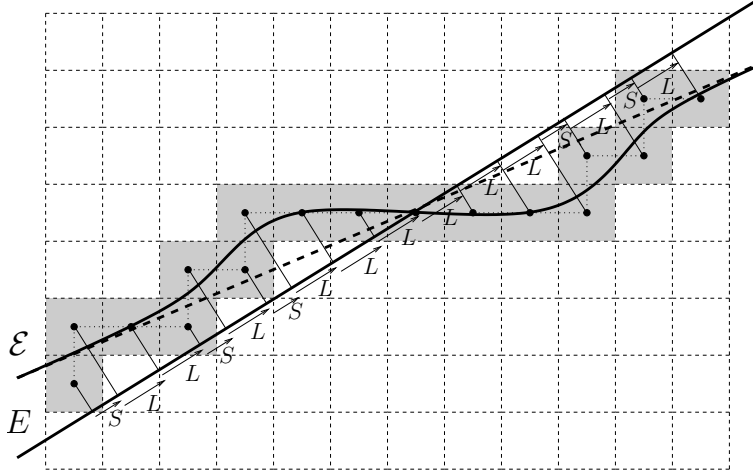


Figure 6: Local excitation of the phasonic degree of freedom for an approximant of the Fibonacci-chain. The excitation rearranges the sequence of the tiles.

3.1 Restriction to excitable degrees of freedom

In the example of the Fibonacci-chain, a local excitation of the phasonic degree of freedom is shown in figure 6. Because of the displacement the cut line \mathcal{E} now selects different atomic volumes. In the tiling this leads to a local rearrangement of the tiles, called phasonic jumps. In general the excitations are considered small and distributed over a wide tiling region, so that the orientational deviation from the planar cut space is small.

A special case has to be examined separately: If the cut plane of an approximant is parallel to boundaries of atomic volumes, it is possible that a local excitation of phasonic degrees of freedom leads to overlapping tiles. If, for example in the Fibonacci-chain, the cut line of the approximant has slope 0, a local excitation always creates regions of the cut line having positive as well as negative slope. The regions of negative slope lead to overlapping tiles, as shown in figure 3(b) earlier. In such a case, accordingly, local displacements of the cut plane are geometrically not allowed and the phasonic degree of freedom is termed *not excitable*.

With regard to the approximants of the 1.6 nm d-(Al-Pd-Mn) in the five-dimensional model, the phasonic degrees of freedom of the Ξ -phases are not excitable in the directions of \mathbf{e}_3^{5D} and \mathbf{e}_4^{5D} . So for a full description of these phases the three-dimensional hyperspace with basis $\{\mathbf{e}_1^{3D} = \mathbf{e}_1^{5D}, \mathbf{e}_2^{3D} = \mathbf{e}_2^{5D}, \mathbf{e}_3^{3D} = \mathbf{e}_5^{5D}\}$ and only one phasonic degree of freedom is sufficient.

This last phasonic degree of freedom is excitable in the ξ'_n -phases, leading to new phenomena. But it is not excitable in the ξ - and the ξ' -phase. (The cut plane of the ξ' -phase, for example, is parallel to the \mathbf{e}_1^{3D} -axis). So the phases ξ and ξ' behave like normal periodic crystals, having only phononic degrees of freedom.

It is a pleasant aspect of the three-dimensional hyperspace that the construction formalism can easily be visualised. Thus in the next sections we can present the cut plane

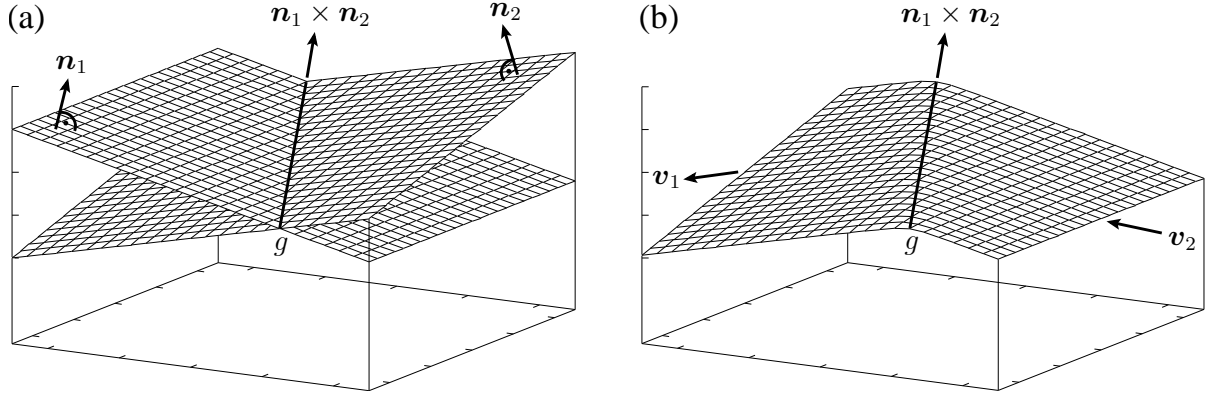


Figure 7: (a) Two different cut planes with normal vectors \mathbf{n}_1 and \mathbf{n}_2 . They have the line g with direction vector $\mathbf{n}_1 \times \mathbf{n}_2$ in common. (b) A transition between the two phases is realised by adjusting the orientation of the cut plane continuously (see text).

for phase boundaries and dislocations as two-dimensional curved surfaces.

3.2 Phasonic phase boundaries

Different approximant phases are characterised by different orientations of the cut space. As a feature of the phasonic degrees of freedom, a spatially dependent continuous transformation from one orientation of the cut space to another is possible, leading to a phasonic phase boundary.

Let two phases be characterised by the normal vectors \mathbf{n}_1 and \mathbf{n}_2 of their cut planes \mathcal{E}_1 and \mathcal{E}_2 (figure 7(a)). For calculating the cut plane \mathcal{E} of the phasonic phase boundary we choose the coordinate system in a way, that the line $g = \mathcal{E}_1 \cap \mathcal{E}_2$ with direction $\mathbf{n}_1 \times \mathbf{n}_2$ runs through the origin. In the limit far away from g on the side of phase 1 the new cut plane \mathcal{E} contains the vector $\mathbf{v}_1 = \mathbf{n}_1 \times (\mathbf{n}_1 \times \mathbf{n}_2)$, while on the other side \mathcal{E} the vector $\mathbf{v}_2 = \mathbf{n}_2 \times (\mathbf{n}_1 \times \mathbf{n}_2)$. By using a transition function $f : \mathbb{R} \rightarrow [0, 1]$ with properties

$$\lim_{x \rightarrow -\infty} f(x) = 0, \quad \lim_{x \rightarrow \infty} f(x) = 1 \quad \text{and} \quad f(0) = 1/2 \quad (12)$$

the cut plane for the phase boundary \mathcal{E} as shown in figure 7(b) is parametrised by:

$$\mathcal{E} = \left\{ s \frac{\mathbf{n}_1 \times \mathbf{n}_2}{\|\mathbf{n}_1 \times \mathbf{n}_2\|} + t \frac{f(t)\mathbf{v}_2 + (1 - f(t))\mathbf{v}_1}{\|f(t)\mathbf{v}_2 + (1 - f(t))\mathbf{v}_1\|} ; s, t \in \mathbb{R} \right\}. \quad (13)$$

Klein et al. (1996) have taken a transmission electron micrograph of a phasonic phase boundary (figure 8(a)), without interpreting it as such. The phason-lines can be seen as dark contrasts. Phase 1 on the left side is one of the phases $\xi(\alpha)$, $0 \leq \alpha \leq 1$ with $\alpha \approx 0.8$, by which we denote an intermediate phase of a ξ - and a ξ' -approximant. Its cut plane is spanned by $\mathbf{a}_{\xi(\alpha)} = (0, -\alpha, 1)$ and $\mathbf{c}_{\xi(\alpha)} = (1, 0, 0)$. Special cases are: $\xi(0) = \xi$ and $\xi(1) = \xi'$. Phase 2 on the right side is the ξ'_2 -approximant.

The tiling for this phasonic phase boundary from $\xi(0.8)$ to ξ'_2 is calculated as explained above and shown in figure 8(b). For the transition function we used:

$$f(x) = \begin{cases} 0 & , x \leq 0 \\ \frac{\arctan(x)}{\pi} + \frac{1}{2} & , x > 0. \end{cases} \quad (14)$$

In the region of the $\xi(0.8)$ -phase ($x < 0$) the cut plane is flat, since in the $\xi(\alpha)$ -phases the phasonic degree of freedom is not excitable, just as in the ξ - or the ξ' -phase. In the region of the ξ'_2 -phase ($x > 0$) excitations of the phasonic degree of freedom show as bendings of the phason-planes.

As a direct consequence of the hyperspace description the orientation of the phasonic phase boundary is completely determined by the involved approximant phases. On the other side, by observing this orientation we can identify the approximant phases, labelled by the parameter α .

4 Dislocations: Energetic consideration

In quasicrystals and approximants dislocations do exist and are characterised by a unique Burgers vector \mathbf{b} , which now is a vector of the hyperlattice. A dislocation is accompanied by a phonon- and a phason-strain field, due to the phononic part $\mathbf{b}_{\parallel} = \pi_{\parallel}\mathbf{b}$ and the phasonic part $\mathbf{b}_{\perp} = \pi_{\perp}\mathbf{b}$ (π_{\perp} projects on the orthogonal complement of E), respectively, of the Burgers vector. If the phasonic part vanishes, the dislocation is a classical one and can be described without the hyperspace methods. Since the lattice constants of periodic approximants are large, classical dislocations have gigantic Burgers vectors with huge phonon-strains. They are energetically unfavourable and will not be observed.

By extending the linear theory of elasticity to hyperspace (approximating the phasonic degree as continuous), the line energy E of a dislocation grows quadratically with increasing lengths $\|\mathbf{b}_{\parallel}\|$ and $\|\mathbf{b}_{\perp}\|$.⁵ Assuming isotropy in the phononic and phasonic part, E can be expressed as:

$$E = c_{\text{phon}}\|\mathbf{b}_{\parallel}\|^2 + c_{\text{phas}}\|\mathbf{b}_{\perp}\|^2 + c_{\text{coupl}}\|\mathbf{b}_{\parallel}\|\|\mathbf{b}_{\perp}\|. \quad (15)$$

Besides a phononic contribution with elastic constant c_{phon} and a phasonic contribution with c_{phas} , a coupling term is present with c_{coupl} .⁶

For estimating the different contributions in (15) the elastic constants in the approximant phases are assumed to be comparable to those of i-Al-Pd-Mn. For the icosahedral phase the phononic elastic constants have been determined by Amazit et al. (1995) from sound-propagation. The phasonic elastic constants have been measured with neutron and x-ray scattering experiments by Letoublon et al. (2001). From the experimental values it

⁵There is an ongoing discussion whether the elastic energy grows linear (locked state) or quadratically (unlocked state) in the phasonic strain, see the review by Edagawa (2001). However at higher temperatures, when dislocations can form and move, the unlocked state is entropically stabilised.

⁶In several papers the coupling term is neglected, although its appearance is a consequence of the linear theory of elasticity.

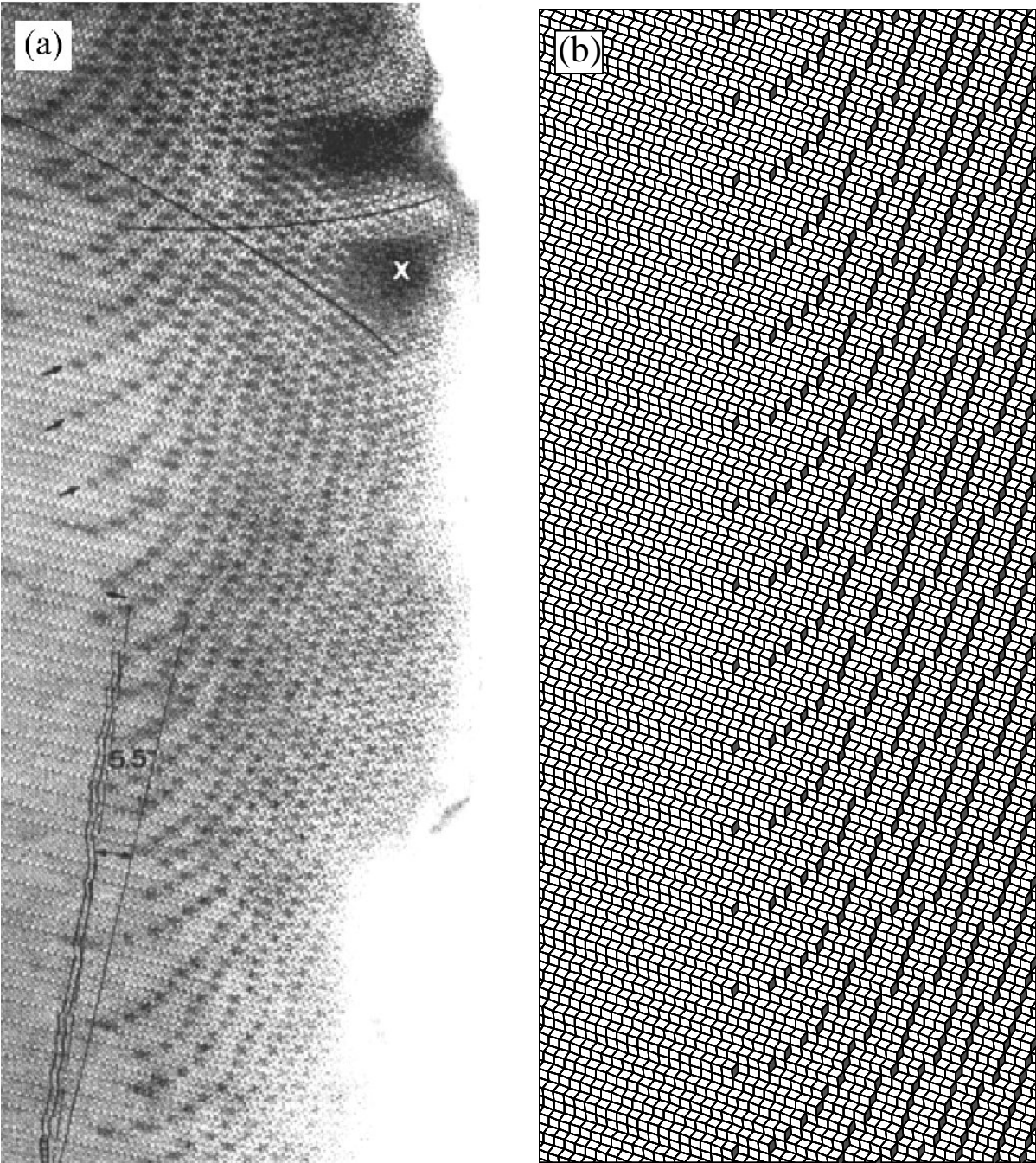


Figure 8: Phasonic phase boundary between the phase $\xi(0.8)$ on the left side and the phase ξ'_2 on the right side. (a) Transmission electron micrograph. The darker spots correspond to phason-lines (Klein et al. 1996). (b) Calculated tiling for the three-dimensional model (see text).

can be concluded, that c_{phas} is a few orders of magnitudes smaller than c_{phon} . Furthermore computer simulations (Koschella et al. 2002) suggest that c_{coupl} has about the same value as c_{phas} . So the largest contribution to E comes from the phononic part. In the tiling picture this means that it is energetically more favourable to rearrange parts of the tiling than to deform tiles.

5 Dislocations in the ξ'_n -phases

The construction method for a dislocation in hyperspace has been discussed e.g. by Bohsung and Trebin (1989). A dislocation with Burgers vector \mathbf{b} forces upon the cut plane a displacement field \mathbf{u} with a phononic and a phasonic part. In a first approximation the displacement field can be distributed isotropically in physical space and becomes in spherical coordinates:

$$\mathbf{u}(r, \varphi) = \frac{\varphi}{2\pi} \mathbf{b}. \quad (16)$$

5.1 Metadislocations in the three-dimensional model

The steps involved in the construction of a dislocation are visualised in figure 9. The distorted cut plane has a strain jump of \mathbf{b}^{3D} along a radial line as shown in figure 9(a). The middle points of the atomic volumes selected by the cut plane form a staircase surface as shown in figure 9(b). This surface is projected with π_{\parallel}^{3D} onto the projection plane (figure 9(c)). Up to now only the phason-strain of the dislocation has been taken regard of and results in a rearrangement of the tiles. The gap in the tiling is caused by the jump line in the cut plane. In a last step the phonon-strain is introduced (figures 9(d), (e)), closing the gap and deforming the tiles. In (figure 9(f)) a Burgers circuit is constructed. The sides of the tiles correspond to projected basis vectors \mathbf{f}_i of the hyperlattice. In the example the lines A, C and B, D cancel each other, only E is left and is lifted to the Burgers vector $\mathbf{b}^{3D} = (-2, 1, -3) = -2\mathbf{e}_1^{3D} + \mathbf{e}_2^{3D} - 3\mathbf{e}_3^{3D}$.

Consider now an arbitrary dislocation with $\mathbf{b}^{3D} = (b_1, b_2, b_3)$, $b_i \in \mathbb{Z}$. Its phononic component

$$\mathbf{b}_{\parallel} = \pi_{\parallel}^{3D} \mathbf{b}^{3D} = \frac{1}{5} \sqrt{10} \begin{pmatrix} \frac{1}{2} \sqrt{\tau + 2} (b_2 - b_3) \\ b_1 + \frac{1}{2} \tau^{-1} (b_2 + b_3) \end{pmatrix}. \quad (17)$$

must be small for low dislocation energy, as shown in the last section. This is achieved, if $b_2 = b_3$ and $\frac{b_2}{b_1} \approx -\tau$. The best approximating rational values for τ are given by fractions $\frac{F_m}{F_{m-1}}$ of successive Fibonacci numbers $(F_m)_{m \in \mathbb{N}} = (1, 1, 2, 3, 5, 8, 13, 21, \dots)$ defined by $F_{m+1} = F_{m-1} + F_m$ with start values $F_1 = F_2 = 1$. They have the following properties, which can be proved by induction:

$$(i) \quad F_m \tau + F_{m-1} = \tau^m \quad (18a)$$

$$(ii) \quad F_{m+1} - F_m \tau = (-\tau)^{-m} \quad (18b)$$

$$(iii) \quad F_m = \frac{1}{5} \sqrt{5} (\tau^m - (-\tau)^{-m}) \quad (18c)$$

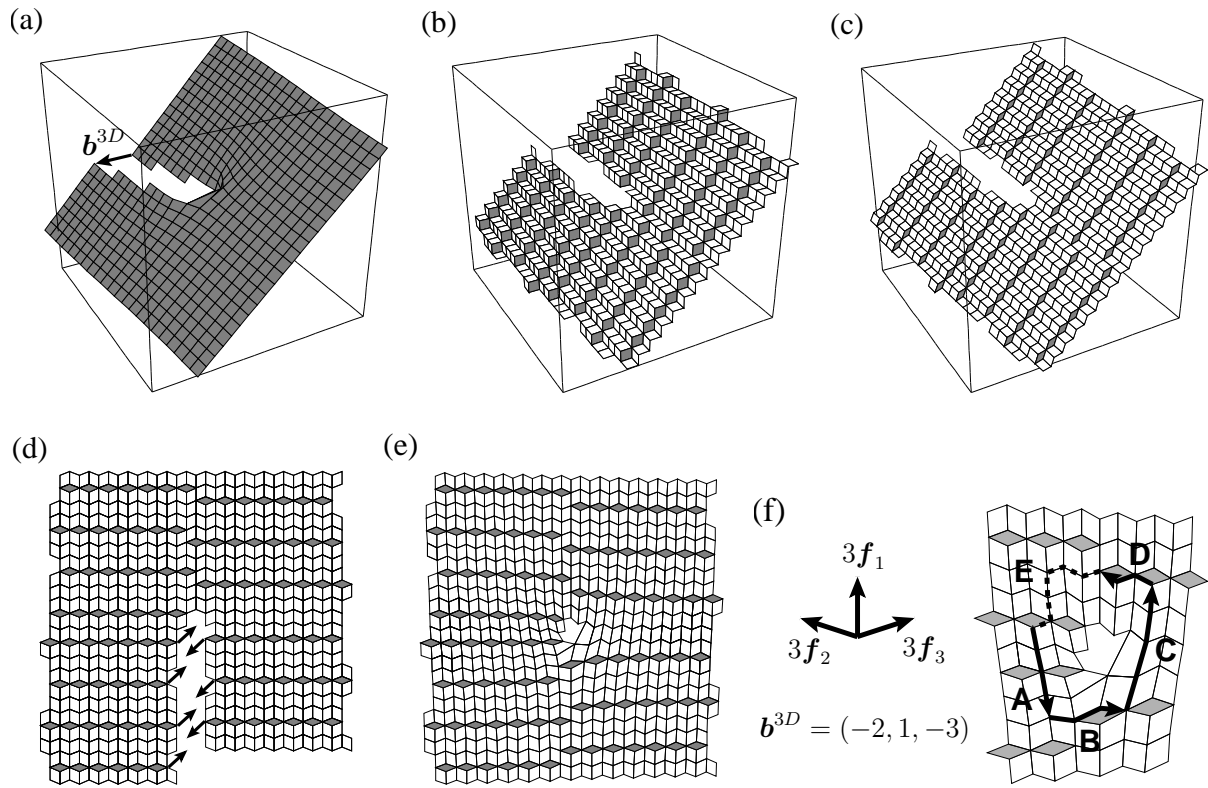


Figure 9: Construction of a dislocation in the three-dimensional model. (a) The displaced cut plane \mathcal{E} of the ξ'_3 -phase around the dislocation core. (b) Staircase surface of those atomic volumes, that are cut by \mathcal{E} . (c) Projection of the staircase surface onto the projection plane E . (d) The new tiling around the dislocation core with rearrangements of the tiles due to phason-strain. (e) The gap in the tiling is closed by phonon-strain. (f) The Burgers vector \mathbf{b}^{3d} can be obtained by performing a Burgers circuit.

Therefore the best candidates for Burgers vectors of low energy dislocations are

$$\mathbf{b}^{3D} = \begin{pmatrix} F_{m-1} \\ -F_m \\ -F_m \end{pmatrix} \quad \text{with} \quad \mathbf{b}_{\parallel} = \frac{1}{5}\sqrt{10} \begin{pmatrix} 0 \\ F_{m-1} - \tau^{-1}F_m \end{pmatrix} \quad (19)$$

and length:

$$\|\mathbf{b}_{\parallel}\| = \tau^{-m} \frac{1}{5} \sqrt{10} l^{3D} = \tau^{-m} \cdot 1.26 \text{ nm}. \quad (20)$$

With (8) and (9) we get the 6D Burgers vector:

$$\mathbf{b}^{6D} = T_{5D}^{6D} T_{3D}^{5D} \mathbf{b}^{3D} = (0, 0, -F_{m-2}, F_{m-1}, F_{m-2}, F_{m-1}). \quad (21)$$

The phasonic component for the six-dimensional hyperspace can be calculated with (18):

$$\begin{aligned} \|\mathbf{b}_{\perp}\| &= \sqrt{\|\mathbf{b}^{6D}\|^2 - \|\mathbf{b}_{\parallel}\|^2} = \sqrt{2[(F_{m-1})^2 + (F_{m-2})^2] (l^{6D})^2 - \frac{2}{5} \tau^{-2m} (l^{3D})^2} \\ &= \tau^{m-3} \frac{1}{5} \sqrt{10} l^{3D} = \tau^{m-3} \cdot 1.26 \text{ nm}, \end{aligned} \quad (22)$$

yielding the strain accommodation parameter ζ , i.e. the ratio of the phasonic and the phononic component of the Burgers vector (Feuerbacher et al. 1997):

$$\zeta = \frac{\|\mathbf{b}_{\perp}\|}{\|\mathbf{b}_{\parallel}\|} = \tau^{2m-3}. \quad (23)$$

Tilings for dislocations with $m = 4$ and $m = 5$ are shown in figures 10(a) and (c). The dislocation cores appear as triangles which can be used for Burgers circuits. Phason-planes come in from the left side of the tiling, ending at the flat side of the triangle, their number being equal to that of the tiles there, which is $2F_m$. Whereas the phononic part of the Burgers vector is much smaller than the side length l^{3D} of the rhombs, the phasonic part is so large that it leads to a bending of the phason-planes over a huge area of the tiling.

The arrangement of the phason-lines can be viewed as a metastructure which, in the simple case of a dislocation free ξ'_n -phase is a striped centred rectangular lattice. A partial dislocation in the tiling leads to a dislocation in the striped metastructure, named metadislocation. A dislocation with a three-dimensional Burgers vector as in (19) is called metadislocation of type m . In contrary to the dislocation constructed in hyperspace, a metadislocation is an ordinary dislocation in the metastructure with a two-dimensional Burgers vector.

The Burgers vector \mathbf{b}_{meta} of a type m metadislocation is oriented in the direction of the lattice vector $\mathbf{c}_{\xi'_n} = \pi_{\parallel}^{3D} \mathbf{c}_{\xi'_n}^{3D}$. Since a lattice cell contains two phason-planes, a type m metadislocation has F_m inserted rows of lattice cells in this direction, leading to a Burgers vector

$$\mathbf{b}_{\text{meta}} = F_m \pi_{\parallel}^{3D} \mathbf{c}_{\xi'_n}^{3D} = \frac{F_m}{5} \sqrt{10} \begin{pmatrix} 0 \\ 2n + \tau^{-1} \end{pmatrix} \quad (24)$$

of length

$$\|\mathbf{b}_{\text{meta}}\| = l^{3D} F_m (2n + \tau^{-1}) = F_m (2n + \tau^{-1}) \cdot 1.26 \text{ nm}. \quad (25)$$

The most frequent dislocations are the type 4 metadislocations in the ξ'_2 -phase. They have been observed by electron microscopy (Klein et al. 1999), see figure 10(b). From our theory we derive the lengths $\|\mathbf{b}_{\parallel}\| = 0.184 \text{ nm}$ and $\|\mathbf{b}_{\perp}\| = 2.04 \text{ nm}$ ($\zeta = 11.1$) for the dislocation and $\|\mathbf{b}_{\text{meta}}\| = 17.5 \text{ nm}$ for the metadislocation, which is larger by two orders of magnitude. For comparison we present the metadislocation also in the hexagon/pentagon/nonagon-tiling (figure 10(d)). Transmission electron micrographs of type 3, 5 and 6 metadislocations have been published, too, by Klein and Feuerbacher (2003).

5.2 Metadislocations in the five-dimensional model

Other kinds of metadislocations reported by Klein and Feuerbacher (2003) also show a large scale arrangement of phason-lines, but require the five-dimensional hyperspace for description, since phason-lines occur in more than one orientation. Here we will discuss two different types of metadislocations:

1. Metadislocations with Burgers vector of the form: $\mathbf{b}^{5D} = (F_m, -F_{m-1}, F_m, 0, 0)$: The phononic component is:

$$\mathbf{b}_{\parallel} = \pi_{\parallel}^{5D} \mathbf{b}^{5D} = \frac{1}{5} \sqrt{10} (-\tau)^{-m} \begin{pmatrix} \cos(72^\circ) \\ \sin(72^\circ) \end{pmatrix}. \quad (26)$$

with length $\|\mathbf{b}_{\parallel}\| = \tau^{-m} \cdot 1.26 \text{ nm}$. The Burgers vector is rotated by 72° compared to the metadislocation in (19). A tiling of such a metadislocation with $m = 3$ is shown in figure 11(a). Phason-lines now appear in two different orientations. F_m rows of tilted phason-lines ending at the dislocation core cannot be explained within the three-dimensional model.

2. Metadislocations with Burgers vector of the form: $\mathbf{b}^{5D} = (0, F_{m-1}, F_{m-1}, 0, F_m)$: The phononic component is:

$$\mathbf{b}_{\parallel} = \frac{1}{5} \sqrt{10} (-\tau)^{-m-1} \begin{pmatrix} \cos(-72^\circ) \\ \sin(-72^\circ) \end{pmatrix}. \quad (27)$$

with length $\|\mathbf{b}_{\parallel}\| = \tau^{-m-1} \cdot 1.26 \text{ nm}$. A tiling with $m = 5$ is shown in figure 11(b). This time F_{m-1} rows of tilted phason-lines end at the dislocation core.

For transmission electron micrographs of the two discussed metadislocations see figure 11(c) and (d). In the first figure the gap extending to the left in the tiling has been closed by the motion of the phason-planes. In the second figure the metadislocation seems to have moved up, while building a sack-shaped area of ξ' -phase below. On the sides of this area, five phason-planes are cut into halves by a region of ξ' -phase.

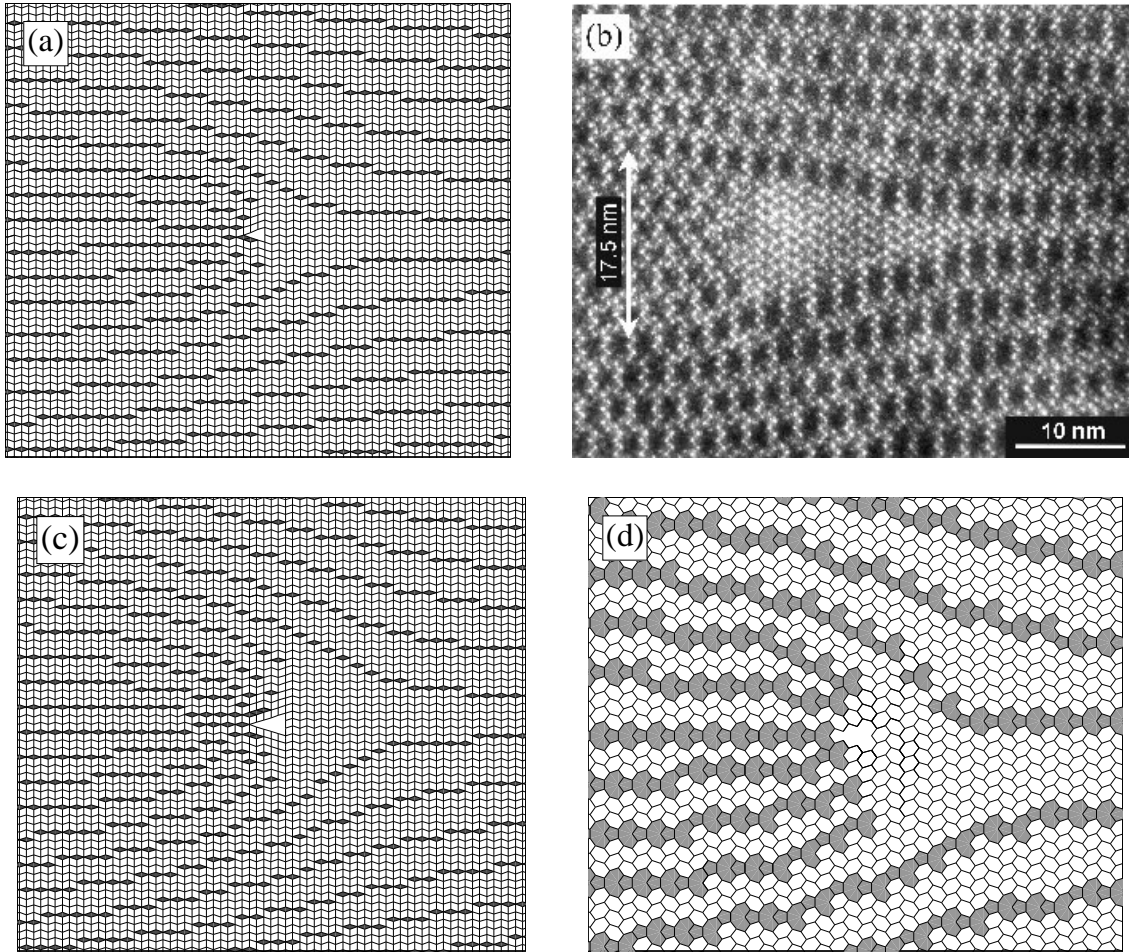


Figure 10: (a) Tiling of a type 4 metadislocation in the ξ'_4 -phase. (b) Transmission electron micrograph of a type 4 metadislocation in the ξ'_2 -phase, courtesy by H. Klein and M. Feuerbacher. (c) Tiling of a type 5 metadislocation in the ξ'_4 -phase. (d) For comparison the calculated hexagon/pentagon/nonagon tiling of a type 4 metadislocation in the ξ'_4 -phase is shown.

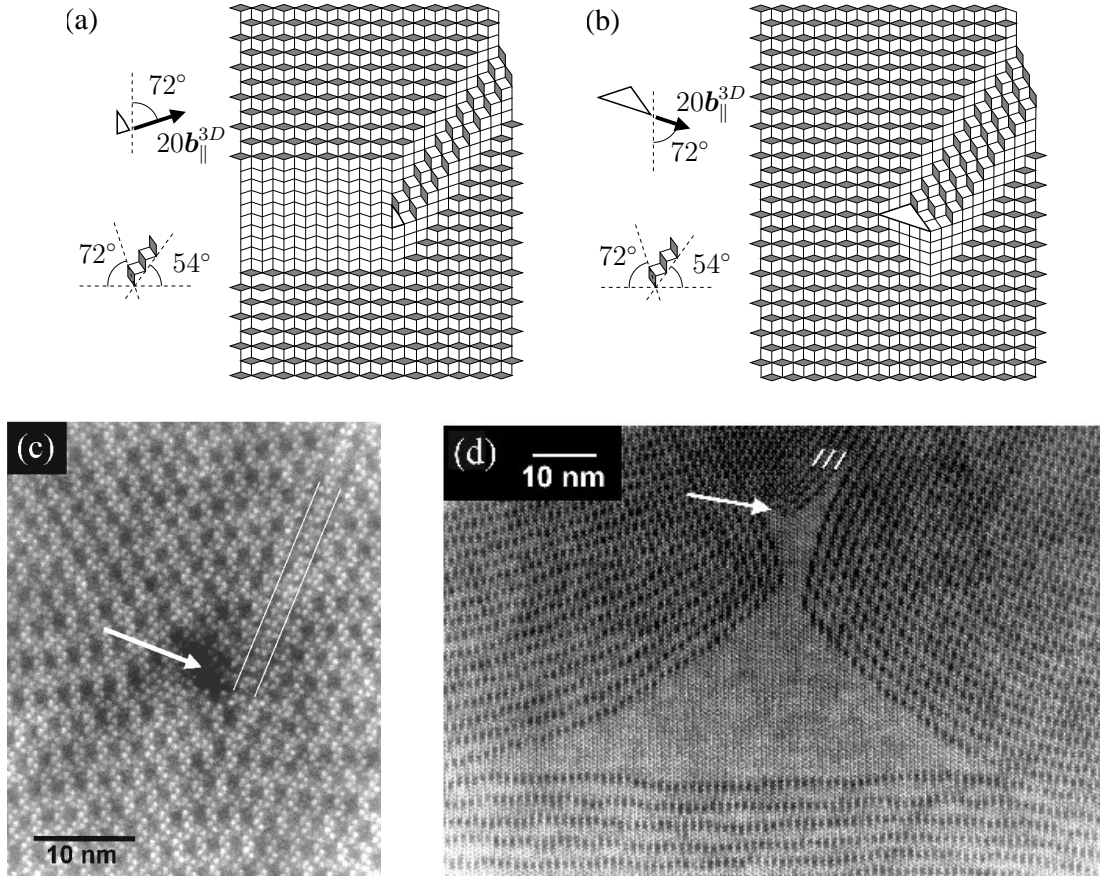


Figure 11: Tilings of metadislocations in the ξ_1^I -phase with Burgers vectors (a) $\mathbf{b}^{5D} = (2, -1, 2, 0, 0)$ and (b) $\mathbf{b}^{5D} = (0, 3, 3, 0, 5)$. The phason-strain field is not distributed isotropic. The phasonic component of the Burgers vector is drawn magnified 20 times, since it is too small otherwise. (c) and (d) show transmission electron micrographs of these two metadislocations, courtesy by H. Klein and M. Feuerbacher.

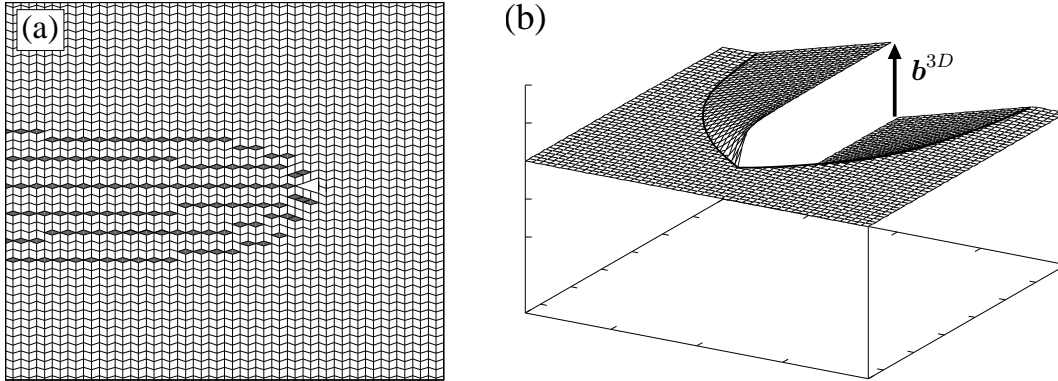


Figure 12: (a) A tiling of a metadislocation in the ξ' -phase with six inserted phason-planes. In the dislocation tail a strip of ξ'_3 -phase is created. (b) Cut plane for the metadislocation in the ξ' -phase. The phason-strain field is not relaxed isotropic, but concentrated in the dislocation tail, where the phason-lines are observed.

6 Metadislocations in the ξ' -phase

Although phasonic degrees of freedom are not excitable *continuously* in the ξ' -phase, metadislocations with phasonic components, which cause a *noncontinuous* local phason-strain do exist and have been observed experimentally by Klein and Feuerbacher (2003). They can be described in the three-dimensional hyperspace. To minimise the dislocation energy, their Burgers vectors \mathbf{b}^{3D} are the same as in the ξ'_n -phases (19). For a tiling see figure 12(a) in the case $m = 4$. Similar to metadislocations in the ξ'_n -phases, a tail of six inserted phason-planes ends at the flat sides of the dislocation core. Towards the dislocation core the phason-planes converge, while far away they run parallel. Contrary to metadislocations in the ξ'_n -phases the phason-strain now is not distributed isotropically around the dislocation core, but concentrated in the region, where phason-lines are observed.

The shape of the cut plane for the metadislocation in the three-dimensional model is shown in figure 12(b), where the coordinate system is rotated, so that the cut plane $\mathcal{E}_{\xi'}$ of the ξ' -phase lies horizontally. Because of its small phononic component, the Burgers vector is almost perpendicular to $\mathcal{E}_{\xi'}$.

We place the dislocation in the origin and the strain jump of \mathbf{b}^{3D} along the y -axis, along a line in the middle of the strip of phason lines. Inside the dislocation tail and far away from the core the strain field is

$$\mathbf{u}^{3D}(x, y) = \frac{x}{2} \left(\frac{1}{|x|} - \frac{1}{\lambda} \right) \mathbf{b}^{3D}. \quad (28)$$

The parameter λ controls the width of the dislocation tail. To simulate a convergence of the dislocation tail $\lambda = \lambda(y)$ must be designed decreasing with distance from the dislocation core. Outside of the dislocation tail, the cut plane is parallel to $\mathcal{E}_{\xi'}$. The region with the phason lines can be viewed as a very thin strip of newly created ξ'_n -phase, embedded in

surrounding ξ' -phase. We suggest, that these dislocations move in the direction of their tail, because for the movement perpendicular to it the entire tail would have to be dragged along. The movement is pure climb, because it is perpendicular to the burgers vector and the dislocation line. There are indications (Momprou, Caillard, and Feuerbacher 2004), that in the i-Al-Pd-Mn quasicrystal dislocations can move by pure climb. Furthermore the most often observed dislocations in i-Al-Pd-Mn have the same burgers vectors as the metadislocations in the Ξ -phases (Rosenfeld et al. 1995).

Finally it should be mentioned that Feuerbacher and Caillard (2004) also observed other dislocations in the ξ' -phase with Burgers vectors that do not lie perpendicular to the vector $\mathbf{b}_{\xi'}^{6D}$. These cannot be pictured as two-dimensional tilings, but require a true three-dimensional description in physical space.

7 Conclusion

In this paper we have introduced a simple projection formalism in five-dimensional hyperspace for the description of the i-(Al-Pd-Mn) approximants ξ , ξ' and ξ'_n as two-dimensional tilings. The tilings correspond to the projections of clusters columns. In most cases the formalism can even be restricted to a three-dimensional hyperspace. The tilings are generated by cuts and projections through a hyperspace which is partitioned into atomic hypervolumes.

We have shown that phasonic degrees of freedom in form of continuous displacements of the cut space do exist in these phases and can be either excitable or not. They play a fundamental role for phasonic phase boundaries as well as dislocations. In the case of the ξ - and ξ' -phase no phasonic degrees of freedom are excitable, while in the ξ'_n -phases there is exactly one excitable phasonic degree of freedom, which is connected to the bending of the phason-planes.

Nevertheless metadislocations in the ξ' -phase can exist, creating phason-planes and forming a thin strip of ξ'_n -phase in their tails while moving by climb. In this way, a consecutive motion of metadislocations through the ξ' -phase induces a phase transformation to a ξ'_n -phase, making the phasonic degree of freedom excitable. The same metadislocations continue to exist in the ξ'_n -phases.

It is possible that phasonic degrees of freedom and dislocations with phasonic components also occur in various other complex metallic alloys, that have connections to quasiperiodic phases. Thus restrictions for ordinary dislocations, that are imposed by the large unit cells, can be overcome.

References

- AMAZIT, Y., FISCHER, M., PERRIN, B., and ZAREMBOWITZ, A., 1995, *Proceedings of the 5th International Conference on Quasicrystals*, edited by C. Janot and R. Mossieri (Singapore: World Scientific), p.584.

- BERAHA, L., DUNEAU, M., KLEIN, H., and AUDIER, M., 1997, *Phil. Mag. A*, **76**, 587.
- BOHSUNG, J., and TREBIN, H.-R., 1989, *Introduction to the Mathematics of Quasicrystals*, edited by M.V. Jarić (London: Academic Press), p.183.
- BOUDARD, M., KLEIN, H., DE BOISSIEU, M., AUDIER, M., and VINCENT, H., 1996, *Phil. Mag. A*, **74**, 939.
- DUNEAU, M., and AUDIER, M., 1994, *Lectures on quasicrystals*, edited by F. Hippert and D. Gratias (Les Ulis: Les Editions de Physique), p. 283.
- EDAGAWA, K., 2001, *Mater. Sci. Eng.*, **A309**, 528.
- FEUERBACHER, M., and CAILLARD, D., 2004, *Acta Mater.*, **52**, 1297.
- FEUERBACHER, M., METZMACHER, C., WOLLGARTEN, M., URBAN K., BAUFELD, B., BARTSCH, M., and MESSERSCHMIDT, U., 1997, *Mater. Sci. Eng.*, **A233**, 103.
- FRENKEL, D.M., HENLEY, C.H., and SIGGIA, E.D., 1986, *Phys. Rev. B*, **34**, 3649.
- GRATIAS, D., KATZ, A., and QUIQUANDON, M., 1995, *J. Phys. Cond. Matter*, **7**, 9101.
- KATZ, A. and DUNEAU, M., 1986, *J. Phys. France*, **47**, 181.
- KATZ, A. and GRATIAS, D., 1994, *Lectures on quasicrystals*, edited by F. Hippert and D. Gratias (Les Ulis: Les Editions de Physique), p. 187.
- KLEIN, H., 1997, PhD Thesis, Institut National Polytechnique de Grenoble, France.
- KLEIN, H., AUDIER, M., BOUDARD, M., DE BOISSIEU, M., BERAHA, L., and DUNEAU, M., 1996, *Phil. Mag. A*, **73**, 309.
- KLEIN, H., DURAND-CHARRE, M., and AUDIER, M., 2000, *J. All. Comp.*, **296**, 128.
- KLEIN, H., and FEUERBACHER, M., 2003, *Phil. Mag.*, **83**, 4103.
- KLEIN, H., FEUERBACHER, M., SCHALL, P., and URBAN, K., 1999, *Phys. Rev. Lett.*, **82**, 3468.
- KOSCHELLA, U., GÄHLER, F., ROTH, J., and TREBIN, H.-R., 2002, *J. All. Comp.*, **342**, 287.
- LÉTOUBLON, A., DE BOISSIEU, M., BOUDARD, M., MANCINI, L., GASTALDI, J., HENNION, B., CAUDRON, R., and BELLISSENT, R., 2001, *Phil. Mag. Lett.*, **81**, 273.
- MOMPIOU, F., CAILLARD, D., and FEUERBACHER, M., 2004, *Phil. Mag.*, **84**, 2777.
- ROSENFELD, R., FEUERBACHER, M., BAUFELD, B., BARTSCH, M., WOLLGARTEN, M., HANKE, G., BEYSS, M., MESSERSCHMIDT, U., and URBAN, K., 1995, *Phil. Mag. Lett.*, **72**, 375.
- SOCOLAR, J.E.S., LUBENSKY, T.C., and STEINHARDT, P.J., 1986, *Phys. Rev. B*, **34**, 3345.
- SUN, W. and Hiraga, K., 1996, *Phil. Mag. A*, **73**, 951.
- TSAI, A.P., YOKOYAMA, Y., INOUE, A., and MASUMOTO, T., 1991, *J. Mater. Res.*, **6**, 2646.